Nano Energy 72 (2020) 104672

Contents lists available at ScienceDirect

Nano Energy

journal homepage: http://www.elsevier.com/locate/nanoen

Ultra-flexible nanofiber-based multifunctional motion sensor

Md. Mehebub Alam [1], Sol Lee [1], Minje Kim, Kyung Seok Han, Viet Anh Cao, Junghyo Nah [**]

Department of Electrical Engineering, Chungnam National University, Daejeon, 34314, South Korea

ARTICLE INFO

Keywords:
Electrospun nanofiber
Triboelectric sensing
Vapor phase polymerization
Piezoresistive sensor

ABSTRACT

Recently, human motion and respiration monitoring sensors have attracted significant research attention in the field of wearable electronics and healthcare applications. Fiber-based electronic sensors demonstrate significant potential for such applications due to their flexibility. However, the superior flexibility of fiber-based sensors is generally limited due to the partial use of rigid elements such as metal electrode layers. In this paper, a simple method is presented for the fabrication of all-nanofiber multifunctional sensors, which consist of triboelectric (TE), piezoresistive (PR), and thermoresistive (TR) sensing elements and demonstrate superior flexibility, excellent wearability, and multifunctionality. The TE sensing unit was fabricated by integrating two triboelectrically dissimilar nanofiber surfaces using a polymer mesh separator, for the formation of internal macroscale air gaps; followed by the electrical polarization of nanofibers. The TR and PR sensing elements were realized using vapor-phase polymerized fiber electrode layers. Using the sensor developed in this study, different motions and breathing frequencies can be individually or simultaneously detected using the TE, PR, and TR sensing elements. This work therefore presents a novel scheme for human motion sensors and breathing sensors, which are widely applicable to wearable electronics, healthcare monitoring, and human-machine interfaces.

1. Introduction

In advent of the Internet of Things (IoT) environment, the real-time monitoring of human body movements or physiological signals is critical for the development of different healthcare applications, which require various wearable sensors [1–4]. Various types of sensors, exploiting resistive [5], capacitive [6] piezoelectric/triboelectric [7,8] and other effects [9–12] have been developed in the past years. Resistive type sensor is suitable for multiparameter sensing under different stimuli, including but not limited to pressure/strain (e.g., piezoresistive sensor), temperature (e.g., thermoresistive sensor). One the other hand, piezoelectric/triboelectric sensors can function in self-powered mode without any external power supply [13,14]. In general, these sensors are usually employed to detect single target signal, but recently there is a growing interest in multifunctional sensors and especially in wearable applications. For instance, Liao et al. reported a multifunctional sensor for detecting strain/temperature/UV [15]. Multifunctional wearable sensor for *in-situ* monitoring of human motion/sweat and physiological signals/volatiles organic compound biomarkers have also been demonstrated by Xu et al. [16,17]. One of the major requirements for these sensors is significant flexibility, as they are directly or indirectly attached on human body. Although numerous flexible sensors have been developed, their flexibility limited by the rigidity of the platforms or active sensing elements employed [18–20]. To overcome this limitation, non-woven nanofiber based wearable sensors have been extensively investigated [21–23]. Given that polymer nanofibers are the main constituents of the sensors, the sensors can be air-permeable and exhibit significant flexibility. Moreover, nanofiber-based sensors require a rigid metallic electrode layer; thus, the flexibility of the devices may be limited. In addition, the metallic electrode layer may be subject to corrosion [24,25]. Therefore, it is necessary to investigate and develop sensors that consist only of polymeric nanofibers, for wearable applications. Another issue with respect to wearable sensor applications is the decrease in power consumption and the integration of multiple functionalities. Due to the limited space available for the integration of the energy storage units in wearable devices, the power required to operate the sensing elements should be reduced. It is therefore necessary to implement self-powered sensor units that utilize piezoelectric or triboelectric electricity generation mechanisms [26,27]. In particular, the triboelectric generation mechanism utilizing frictional triboelectrification and electrostatic induction has attracted significant research attention with respect to the harvesting of energy from human

* Corresponding author.
E-mail address: jnah@cnu.ac.kr (J. Nah).
[1] These authors are contributed equally.

https://doi.org/10.1016/j.nanoen.2020.104672
Received 14 January 2020; Received in revised form 21 February 2020; Accepted 3 March 2020
Available online 6 March 2020

body motion, which can also be used as a self-powered sensing element [28–33]. However, in the case of triboelectric sensing and power generation, it is difficult to integrate two triboelectrically different friction surfaces into a single device, given that a minimum separation distance is required for contact and separation motion [34,35]. Therefore, it may be more difficult to integrate a triboelectric sensing unit and other sensors into the ultra-flexible platform, which only consists of nanofibers. It is therefore necessary to develop a facile method for the realization of ultra-flexible fiber-based sensors with integrated multifunctionalities. In this regard, electrospinning is found to be a facile way to fabricate different polymer nanofibers, metal–organic frameworks (MOFs) [36,37], transition metal oxides (TMOs) [38], composites for energy storage and conversion applications [39,40].

This paper presents an ultra-flexible multifunctional sensor that consists only of electrospun nanofibers, for the sensing of human motions and breathing frequencies. By adopting an ultrathin polymeric mesh separator, two triboelectrically different friction surfaces (PVDF-TrFE and PU fibers) on the fiber electrode layers were integrated into a single device with a minimal separation gap. The TE sensing unit can effectively convert various human motions into electrical output signals. Thus, it can function as a sensing device and a biomechanical energy harvesting device. Moreover, a vapor-phase polymerized electrospun fiber electrode was employed as the piezoresistive (PR) sensing element and thermoresistive (TR) sensing element. Using multiple sensing units that consist of TE, PR, and TR elements, different human motions and breathing states have been successfully detected and identified. This paper proposes a novel device structure and approach for the development of ultra-flexible human motion and breathing sensors, which serves as a basis for the further development of wearable sensors.

2. Results and discussion

A schematic illustration is presented in Fig. 1a–c, which describes the fabrication procedures of the triboelectric sensing unit. The poly [(vinylidenefluoride-co-trifluoroethylene)] (PVDF-TrFE) solution was electrospun on a polypropylene mesh, as described in Fig. 1a. Moreover, the PVDF-TrFE solution was loaded into a 10 mL syringe with a metal needle tip, and then ejected through the tip by a syringe pump at a constant flow rate of 1.5 mL/h; facilitated by an electric field formed between the tip and the collector plate, which were separated by a distance of 12 cm. Given that the solution in the syringe was ejected from the tip, solid fibers were formed on the polypropylene (PP) mesh due to solvent evaporation in the solution. The fibers are shown in the corresponding SEM images, where the average fiber diameter was found to be ~1 μm, as shown in Fig. S1(a, i). The PVDF-TrFE fibers on the mesh were employed as the negative friction layer for triboelectric nanogenerators (TENGs), as shown in Fig. 1b. As a positive friction layer, a polyurethane (PU) solution was electrospun on the mesh in a similar manner, and the corresponding SEM of the PU fiber is shown in Fig. 1c. The average fiber diameter was found to be 1.5 μm, as shown in Fig. S1 (a, ii). The prepared PU fiber mat on the mesh was then flipped vertically (Fig. 1b) and integrated as a positive friction layer. The Fourier transform infrared (FT-IR) spectra shown in Fig. S1(b, i) presents the typical characteristic peaks of each friction layer. The PVDF-TrFE layer exhibited characteristic peaks related to the ferroelectric beta phase; and the PU layer exhibited characteristic peaks, which correspond to C═O, N–H, C–H, and C–O bonding. The overall structure of the fabricated TE sensing element after the integration of the top and bottom electrodes (as-prepared poly(3,4-ethylenedioxythiophene) polystyrene sulfonate

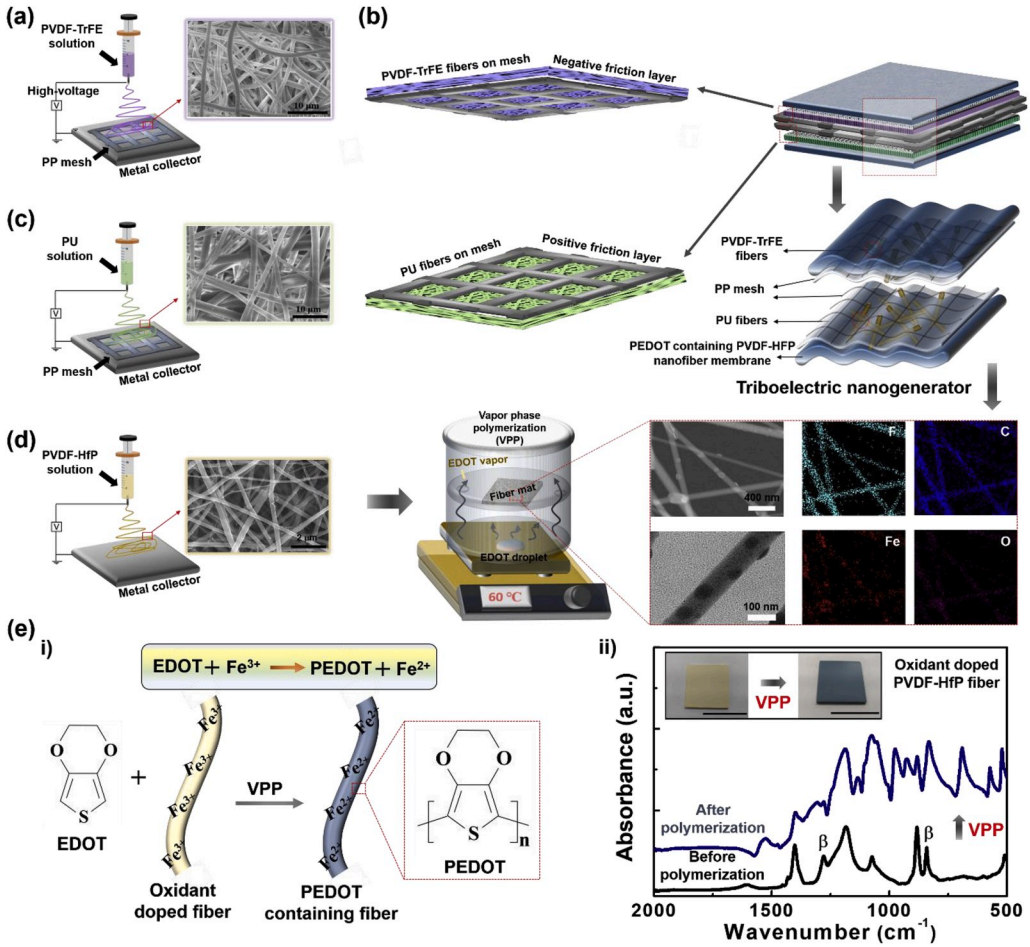

Fig. 1. a) Schematic representation of electrospinning process of PVDF-TrFE, and SEM images of the fibers; in addition to PVDF-TrFE fiber mat on the polypropylene (PP) mesh. b) Structure of the as-prepared TE sensing unit with PVDF-TrFE, PU, PEDOT, which contained the conducting PVDF-HFP nanofiber mat as a negative friction layer, positive friction layer, and electrode layer, respectively, with meshes as the separator. c) Schematic representation of the electrospinning process of PU, and SEM images of the fibers. d) Schematic presentation of electrospinning process of oxidant doped PVDF-HFP, and SEM images of the nanofibers (left). Schematic of VPP process (right). The enlarged view showing the TEM images and EDS mapping of the PEDOT contained PVDF-HFP nanofibers. e) Schematic of VPP reaction mechanism: FT-IR image (scale bar: 2.5 cm) in the inset of the oxidant -doped PVDF-HFP nanofiber mat i) before and ii) after VPP.

(PEDOT)-coated conducting fiber mat) is shown in Fig. 1b. Given that all the layers consist of flexible nanofibers and a thin PP mesh, the device exhibited remarkable flexibility (as shown in Fig. S1(b, ii)), which is critical for the formation of conformal contact with the human body. Thus, the sensors presented in this works are bendable, rollable, twistable, and even foldable, exhibiting ultra-flexibility as demonstrated in other works [41,42]. Moreover, the roles of the PP mesh, as opposed to significant flexibility, are twofold. First, it functions as a supporting layer for electrospun nanofibers. Hence, nanofibers can be collected on the rounded rectangular holes, as shown in Fig. S2a. This also reinforces the mechanical strength of the fiber mat (Fig. S2b). Second, it provides a minimal contact-separation gap (~260 μm), which is necessary for the generation of triboelectric sensing signals by the frictional contact between two different nanofiber layers. The preparation of the electrode layer is described in Fig. 1d. Oxidant-doped (i.e., $FeCl_3.6H_2O$) PVDF-HFP solution was electrospun on a metal collector at a constant flow rate of 0.5 mL/h (Fig. 1d (left)). The as-prepared electrospun fiber mat was then peeled-off from the collector and exposed to the 3,4-ethylenedioxythiophene (EDOT) monomer vapor in a closed vapor-phase polymerization (VPP) chamber (Fig. 1d (right)); where 20 μL of the EDOT monomer was drop-casted at the bottom surface, and the entire chamber was maintained at 60 °C during the VPP process. The EDOT was vapor-polymerized to PEDOT when passed through the oxidant-doped PVDF-HFP fiber mat; thus, the PEDOT-doped conducting nanofiber mat was obtained. Thereafter, it was washed using deionized (DI) water to remove the unreacted oxidant and an EDOT monomer, and then dried in air. The vapor-phase polymerization mechanism is presented in Fig. 1(e, i). When the EDOT monomers were in contact with the oxidant-doped PVDF-HFP fibers, the EDOT monomers lost an electron to Fe^{3+} of $FeCl_3$ and transformed into free radicals; where Fe^{3+} transformed into Fe^{2+}, and the EDOT radicals polymerized to PEDOT [43]. Indeed, the TEM images in Fig. 1d show that the oxidant is clearly incorporated into the nanofiber after the polymerization process, which is also confirmed by electron dispersive spectroscopy (EDS) mapping. After this polymerization, the color of the fiber mat was a deep bluish color, as shown in the images (the inset of Fig. 1(e, ii), thus verifying the EDOT to PEDOT conversion. The VPP was further confirmed by the FT-IR analysis. Before polymerization, the oxidant containing PVDF-HFP exhibited the typical spectra of ferroelectric beta phase, as shown in Fig. 1(e, ii). After polymerization, all the spectra exhibited the typical bands for PEDOT [44]. Even after six months in the air, there was no change in sheet resistance and the FTIR spectra (Figs. S3a and S3b), which confirms the stability of the PEDOT. Moreover, sufficient power can be supplied to blue light-emitting diode (LED) under the same bias conditions after replacing of the portion of the wire with the PEDOT coated PVDF-HFP electrospun nanofiber mat as shown in Fig. S3c, which has been maintained even after six months in the air.

In this study, the vapor-phase polymerized PVDF-HFP nanofiber layer played dual roles as PR sensing and TR sensing units; thus, its optimization was required. To determine the optimal oxidant content, the sheet resistance of the PEDOT-coated PVDF-HFP mat was measured as a function of the oxidant content, as shown in Fig. 2a. Overall, the sheet resistance of the nanofiber mat decreased in accordance with an increase in the weight percentage of the oxidant (i.e., $FeCl_3$). The sheet resistance rapidly decreased when the oxidant content was higher than 2 wt%: from approximately 3×10^{10} Ω/sq. to 10^3 Ω/sq. The sheet resistance was saturated for oxidant contents greater than 3 wt%. Thus, the PVDF-HFP nanofiber membrance containing 4 wt% for electrode was adopted in this work. The inset Fig. 2a reveal that the fiber mat assumed a darker blue color in accordance with an increase in the oxidant content. To examine the stability and durability of the nanofiber mat, its sheet resistance was examined by conducting the following different types of cyclic deformation tests: bending, rolling, and folding. The results in Fig. 2b reveal that there was a negligible change in the sheet resistance over 1000 cycles of bending tests and more than 100 cycles of rolling and folding tests, thus ensuring its mechanical robustness. Moreover, the thermosensitivity of the conducting mat (i.e., PEDOT-coated PVDF-HFP electrospun fiber mat) was investigated by examining the changes in the electrical resistance at different temperatures. Fig. 2c presents the temperature-dependent resistance changes in

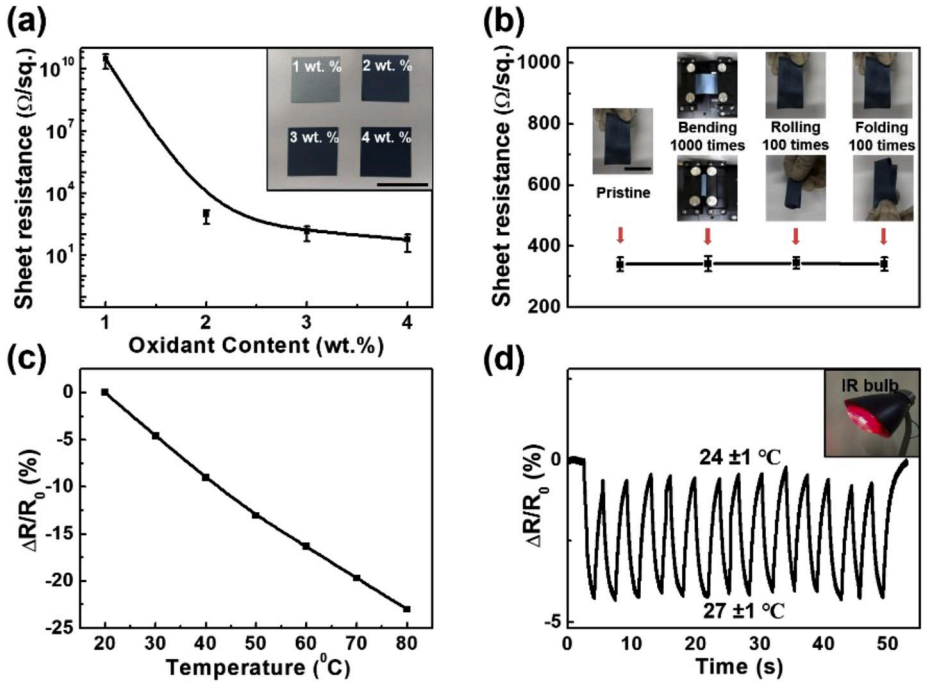

Fig. 2. a) Sheet resistance of VPP PEDOT, which contained the conducting PVDF-HFP nanofiber mat, with respect to the oxidant content; and digital images (scale bar: 2 cm) of each mat shown in the inset. b) Sheet resistance values of the conducting mat after different types of mechanical deformations. c) Changes in the resistance of the conducting mat as with respect to temperature. d) Cyclic temperature tests of the conducting mat due to variations in temperature from 24 to 27 ± 1 °C.

the nanofiber layer, which can be used as TR sensing element. The increase in the carrier concentration by the thermal activation of PEDOT is responsible for the changes in resistance. It should be noted that a linear temperature response was observed for temperatures of up to 80 °C. The nanofiber mat was exposed to irradiation by an infrared lamp (Philips), where the temperature was varied between 24 ± 1 °C and 27 ± 1 °C for multiple cycles, as shown in Fig. 2d. When the lamp was switched ON, the resistance of the fiber mat decreased significantly in accordance with an increase in the concentration of the thermally-activated carrier. On the contrary, when the lamp was switched OFF, there was an abrupt increase in the resistance of the fiber mat. Furthermore, the long term repeatability was measured to confirm stability and durability of PVDF-HFP nanofiber membrane as shown is Fig. S4.

Thereafter, to maximize the performance of the TE sensing unit, the ferroelectric PVDF-TrFE nanofiber layer, which functions as a negative triboelectric friction layer, was electrically polarized. During the electrospinning of the PVDF-TrFE nanofibers, the dipoles of the as-prepared PVDF-TrFE fibers were randomly oriented, which can reduce the net dipole moment due to the dipole cancelation (Fig. 3a). Thus, by polarizing randomly-distributed dipoles in a particular direction, the net dipole moment can be increased. After the polarization of the PVDF-TrFE nanofiber mat in each direction, the triboelectric output voltage was generated by the frictional contact with the PU nanofiber mat with triboelectrically positive properties, as shown in Fig. 3b. The highest output signal was obtained when the PVDF-TrFE nanofiber mat was polarized to exhibit its negative center of dipoles on the frictional surface, which is referred to as 'reverse polarization'. A peak-to-peak output voltage (V_{pp}) of 15 V was obtained before the polarization process. This increased to 23 V after the 'reverse polarization', which corresponds to a 53% increase in the output voltage. However, when the fiber mat was polarized in forward direction, the triboelectric output signal was significantly reduced when compared with the value obtained from the non-polarized fiber mat. The output signal generation mechanism of the TE element is shown in Fig. 3c. When an external force was applied, two triboelectrically opposite fiber surfaces came into contact as the mesh was deformed, and charge transfer occurred between the two fiber layers. Thus, the PVDF-TrFE and PU fibers were negatively and positively charged, respectively. As the two surfaces were separated, the charged fiber surfaces induced opposite charges on the PEDOT-doped conducting nanofibers, thus generating the output signals. In addition, the frictional surfaces were further analyzed using Kelvin prove force microscopy (KPFM) (Fig. 3d and S5). On the one hand, the reverse polarization significantly improved the surface charge of the non-polarized PVDF-TrFE fiber mat from −1.9 V to −2.7 V. On the other hand, the surface potential significantly decreased to −0.9 V after forward polarization. The results are consistent with the results presented in Fig. 3b. The polarity of the PU nanofiber counter friction surface was positive due to the frictional contact with the PVDF-TrFE nanofiber mat. It should be noted that the TE sensing unit generated consistent output signals during the cyclic measurements (Figs. S6 and S7), which have been maintained when measured after six months, ensuring durability and stability of the sensor. Thus, it can also be utilized for biomechanical energy harvesting applications and can generate sufficient power for at least 10 LEDs (Fig. S6d).

After the optimization of the PR and TE sensing units, different motions were detected using the nanofiber device. The inset in Figs. 4(a and b) presents the output signals from the TE sensing and PR sensing units during the folding and unfolding motions; thus indicating the superior flexibility of the proposed device, in addition to the different output signal patterns from both sensing units. During the folding motion, AC output signals were obtained from the TE sensor due to the triboelectric induction mechanism, whereas pulse shaped signals were transmitted from the PR sensor due to changes in resistance; as detected. To further demonstrate the significant applicability of the sensor, it was attached onto the index finger of a human subject for the sensing of pressing and bending finger motions. The results in Figs. 4(c and d) indicate that the PR sensor detected bending motions; however, there was a negligible sensor response to the pushing motion. The TE sensor detected both the pressing and the bending motions, as shown in Figs. 4 (e and f), thus exhibiting different signal patterns for each motion. Moreover, the signals from the TE sensor can be utilized for velocity calculations. The average angular velocity (ω) of the finger motion can also be calculated as $\omega = \phi f_0$; where ϕ and f_0 are the angle and fundamental frequency, respectively. The FFT spectra that represent the fundamental frequencies of the finger motions are shown in the corresponding inset of Fig. 4f. The average velocity was found to be 2.8 rad/s for the finger press motion, whereas an average velocity of 1.2 rad/s was calculated for the bending motion (angle: $45^\circ = \pi/4$). The same motion

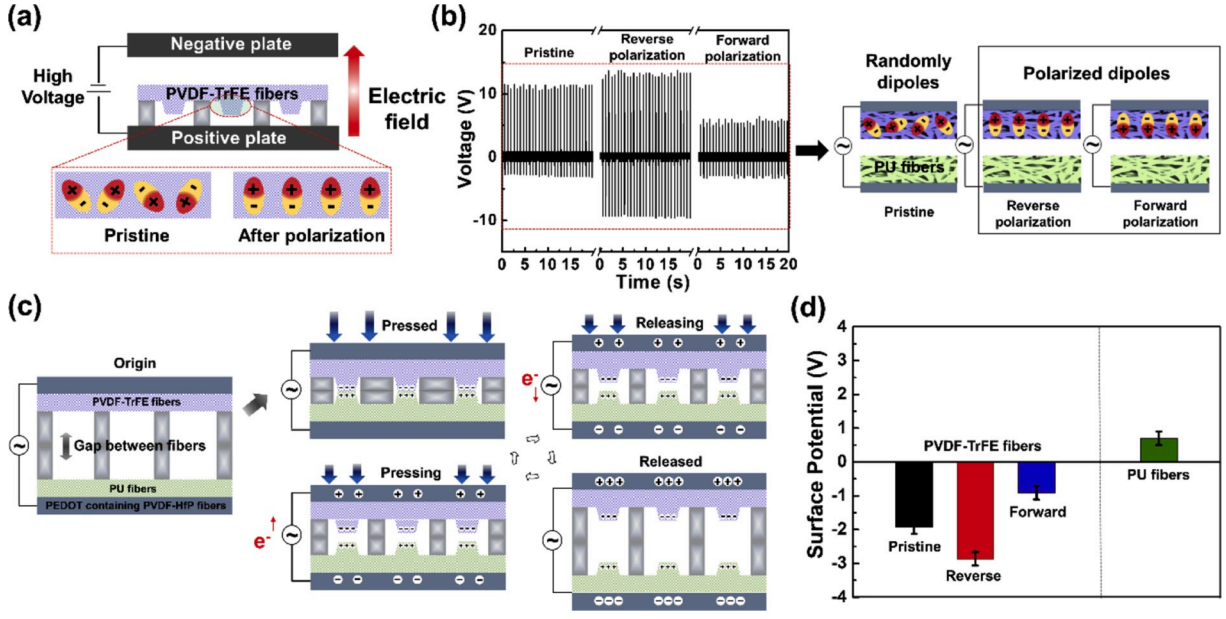

Fig. 3. a) Schematic representation of the polarization process, and enlarged view of dipole orientation of electrospun PVDF-TrFE fibers before and after polarization. b) Output voltage from TENGs with the corresponding device structure (mesh is not shown for simplicity) before and after polarization. c) Schematic representation of operating mechanism of the TENG. d) Surface potential of the PVDF-TrFE (before and after polarization) and PU fiber mats.

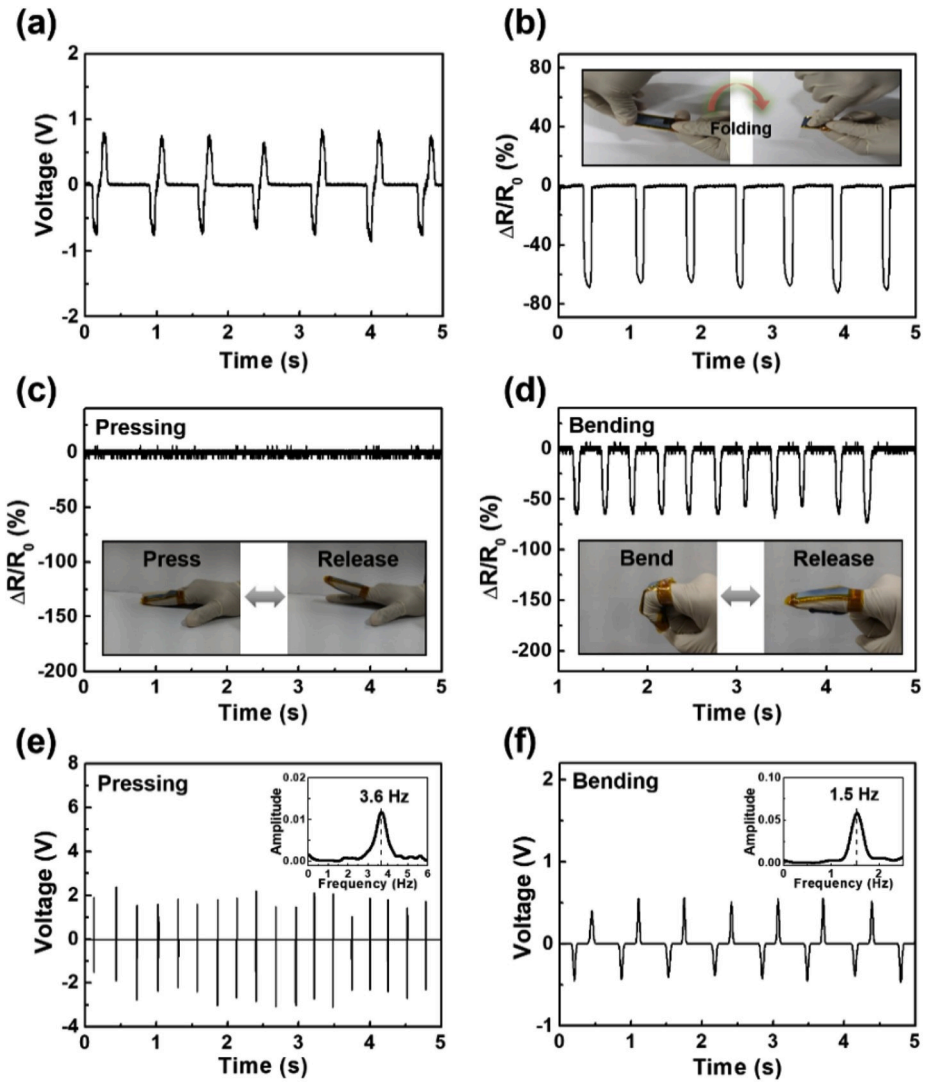

Fig. 4. a) Output voltage signals of TE and b) piezoresistive signal from PR under repeated fold and release conditions. Piezoresistive signal from PR due to c) finger pressing and d) bending motions. The inset images present the corresponding signals due to finger motion. Output voltage signals of the TE due to e) finger pressing and f) bending motions. Inset Figs. present the corresponding FFT spectra.

can therefore be more accurately analyzed and differentiated by simultaneously using multiple sensor responses. Apart from finger motion detection, the TE sensor can also detect wrist motion, elbow motion, foot press and even mouth blowing as shown in Fig. S8.

Similarly, to monitor the human respiration rate, the sensor was attached onto a commercial dust proof mask, as shown in the inset of Fig. 5a. Using the TE sensor, the output signals were measured to determine the number of respiration cycles before and after physical exercise (Figs. 5(a and b)). Given that the sensor is made only of nanofiber layers and a porous PP mesh, the inhalation and exhalation of air can easily penetrate the mesh layer. The TE output signals were generated by frictional contacts between two different TE layers due to the different pressure drops. The respiration frequencies measured using the TE sensing element, as represented by the FFT spectra, were 0.3 Hz and 0.45 Hz at rest and after exercise, respectively (Figs. 5(a and b) insets). Thus, the respiration rate was found to be 18 breaths/min and 27 breaths/min at rest and after exercise, respectively. It should be noted that the respiration rate for healthy adults at rest is 12–20 breaths/min. Similarly, the respiration rate can also be obtained from the TR sensing element. During the inhalation and exhalation of air, there were changes in the temperature inside the mask, thus resulting in changes in resistance. Thus, the respiration rates at rest and after exercise were also measured using the TR sensing unit (Figs. 5(c and d)). The respiration rates measured from the TR sensing unit were in good agreement with the triboelectrically-measured data shown in Figs. 5(a and b). Along with the monitoring of the respiration rate, the TR sensor can also be employed for the monitoring of human body temperature. Therefore, physiological information can be more accurately analyzed and evaluated by the simultaneous acquisition of the TE and the TR sensing data.

3. Conclusion

In this study, an ultra-flexible electrospun nanofiber-based sensor with triboelectric, piezoresistive, and thermoresistive sensing capabilities was developed. The nanofiber-based TE sensor was realized by merging two different triboelectric friction layers on the mesh, which provided a minimal separation gap for triboelectric charge induction. The PEDOT containing PVDF-HFP nanofiber layer serves as a flexible electrode as well as PR and TR sensors. Therefore, fiber-based organic polymer electrodes offer the opportunity to fabricate multifunctional sensors that can meet the primary requirements of wearable sensors that are flexible, lightweight, skin-adhesive and air-permeable. Using the sensor developed in this study, real-time human motion sensing and respiration rate monitoring were successfully demonstrated. The

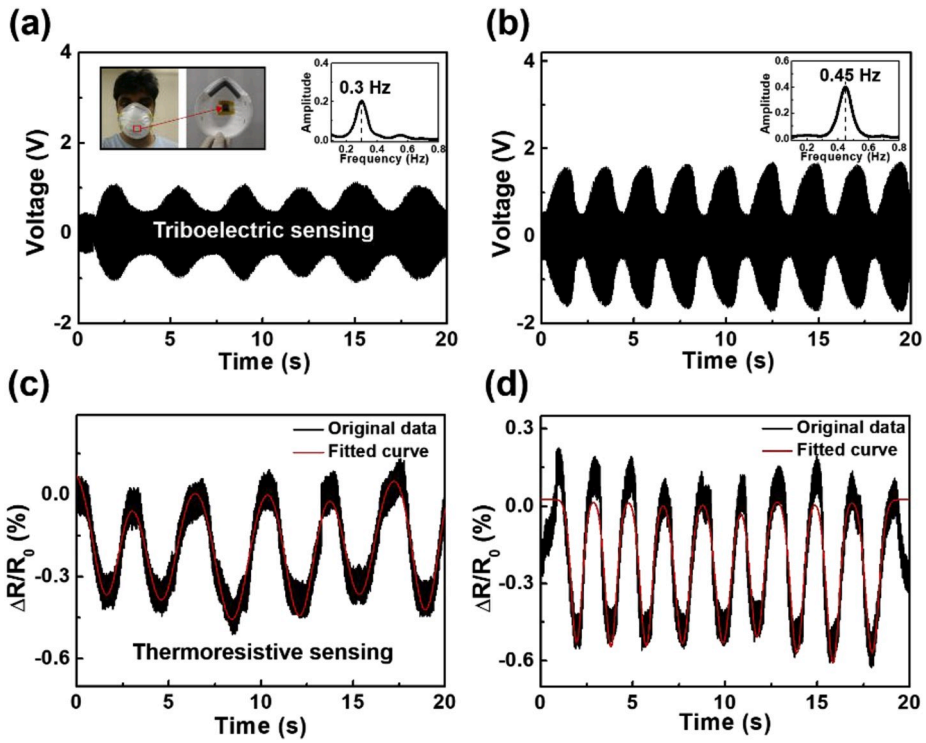

Fig. 5. a) Output voltage signals of TE at normal breathing and b) breathing after exercise with the corresponding FFT spectra in the inset. Inset images (left-side) present the TE attached to a commercial breathing mask. c) The TR signals at normal breathing and d) breathing after exercise.

method employed in this study can serve as a basis for the realization of ultra-flexible wearable sensors for the detection of the multiple physiological signals transmitted by the human body.

4. Experimental section

4.1. Materials

Polyurethane (PU) granules were purchased from Goodfellow (nominal granule side 3–5 mm). Poly (vinylidene fluoride-trifluoroethylene) (PVDF-TrFE) powder with a content of 30% (mol %) was purchased from Piezotech-Arkema Corp. Poly (vinylidene fluoride-*co*-hexafluoropropylene) (PVDF-HFP) was purchased from Goodfellow. 3,4-Ethylenedioxythiophene (EDOT) was purchased from Acros organics and Iron (III) Chloride was purchased from Duksan. All solvents, such as N,*N*-dimethylformamide (DMF), N,*N*-dimethylacetamide (DMAC), Tetrahydrofuran (THF), and acetone, were purchased from Alfa Aesar and Sigma-Aldrich. Polypropylene mesh of thickness of 0.13 mm and hole size of 3 × 2.7 mm^2 was purchased from APEC Industry.

4.2. Triboelectric friction layers and TENG fabrication

For a negative friction layer, 15 wt% PVDF-TrFE solution was prepared in co-solvent of DMF and acetone (1:2 vol ratio) under magnetic stirring at 60 °C for 2h and then electrospun on a polypropylene mesh. For a positive friction layer, 15 wt% PU solution was prepared in co-solvent of DMF and THF (1:2 vol ratio) for electrospun on the mesh. Finally, the ferroelectric negative friction layer was also polarized under high electric field (80 kV/cm) for 1 h using a custom-built electric field driven high voltage poling equipment. The fibers containing meshes are then assembled face to face and electrodes (as prepared PEDOT coated conducting fiber mat) are physically attached on the back side of friction layers. Finally, two mesh layers with different triboelectric properties are glued to function as TENG.

4.3. Electrode layer fabrication

15 wt% (w/v) PVDF-HFP solution was prepared in co-solvent of DMAc and acetone (1:1 vol ratio) under magnetic stirring at 60 °C for 2h. Then, 4 wt% of oxidant (i.e., $FeCl_3.6H_2O$) (w/v) was added and kept stirring for 6h to get a homogeneous solution. It was then electrospun on a metal collector and the as-prepared electrospun fiber mat was then peel-off from the collector and put into EDOT vapor for vapor phase polymerization. After the polymerization it was then dipped in DI water for 30 min and subsequently dried at 60 °C.

4.4. Characterization and measurement

The scanning electron micrograph (SEM) was obtained using S-4800 (Hitachi). The field emission transmission electron microscope (TEM) and electron dispersive spectroscopy (EDS) were obtained using Tecnai G^2 F30 S-TWIN (FEI). The Fourier-transform Infrared Spectroscopy (FT-IR) spectroscopy were performed with Vertex 80/80v (Bruker). The surface potentials were measured by the noncontact mode Kelvin probe force microscopy (Park systems XE 7), where a Pt-coated cantilever was used. The sheet resistance of PEDOT containing PVDF-HFP mats were measured with four-point probe method at room temperature. Agilent 34401A digital multimeter was employed for piezoresistive and thermoresistive sensing tests. The triboelectric outputs were measured by an oscilloscope (Teledyne Wavesurfer 3022) with a 10 MΩ impendence probe.

Declaration of competing interest

The authors declare that they have no known competing financial interests or personal relationships that could have appeared to influence the work reported in this paper.

CRediT authorship contribution statement

Md. Mehebub Alam: Investigation, Writing - original draft. **Sol Lee:** Investigation, Writing - original draft, Writing - review & editing. **Minje Kim:** Formal analysis. **Kyung Seok Han:** Validation. **Viet Anh Cao:** Investigation. **Junghyo Nah:** Conceptualization, Writing - original draft, Writing - review & editing, Writing - review & editing, Funding acquisition.

Acknowledgments

This research was supported by Basic Science Research Program through the National Research Foundation of Korea (NRF-2019R1A2C1010384 and NRF-2020R1A4A2002021), Korea Electric Power Corporation (R18XA06-04), and Samsung Electronics.

Appendix A. Supplementary data

Supplementary data to this article can be found online at https://doi.org/10.1016/j.nanoen.2020.104672.

References

[1] S. Yao, P. Swetha, Y. Zhu, Adv. Healthc. Mater. 7 (2018), 1700889.
[2] Y. Xiong, Y. Shen, L. Tian, Y. Hu, P. Zhu, R. Sun, C.-P. Wong, Nano Energy 70 (2020), 104436.
[3] Z. Zhao, Q. Huang, C. Yan, Y. Liu, X. Zeng, X. Wei, Y. Hu, Z. Zheng, Nano Energy 70 (2020), 104528.
[4] M. Zhu, M. Lou, I. Abdalla, J. Yu, Z. Li, B. Ding, Nano Energy 69 (2020), 104429.
[5] T. Wang, Y. Guo, P. Wan, H. Zhang, X. Chen, X. Sun, Small 12 (2016) 3748–3756.
[6] A. Frutiger, J.T. Muth, D.M. Vogt, Y. Menguc, A. Campo, A.D. Valentine, C. J. Walsh, J.A. Lewis, Adv. Mater. 27 (2015) 2440–2446.
[7] Y. Jie, Q. Jiang, Y. Zhang, N. Wang, X. Cao, Nano Energy 27 (2016) 554–560.
[8] Y. Jie, X. Jia, J. Zou, Y. Chen, N. Wang, Z.L. Wang, X. Cao, Adv. Energy Mater. 8 (2018), 1703133.
[9] S. Bai, C. Sun, H. Yan, X. Sun, H. Zhang, L. Luo, X. Lei, P. Wan, X. Chen, Small 11 (2015) 5807–5813.
[10] T. Wang, Y. Guo, P. Wan, X. Sun, H. Zhang, Z. Yu, X. Chen, Nanoscale 9 (2017) 869–874.
[11] Y. Zhou, M. Zhang, Z. Guo, L. Miao, S.-T. Han, Z. Wang, X. Zhang, H. Zhang, Z. Peng, Mater. Horiz. 4 (2017) 997–1019.
[12] T. Wang, D. Qi, H. Yang, Z. Liu, M. Wang, W.R. Leow, G. Chen, J. Yu, K. He, H. Cheng, Y.L. Wu, H. Zhang, X. Chen, Adv. Mater. 31 (2019), 1803883.
[13] X. Cao, Y. Jie, N. Wang, Z.L. Wang, Adv. Energy Mater. 6 (2016), 1600665.
[14] Y. Jie, H. Zhu, X. Cao, Y. Zhang, N. Wang, L. Zhang, Z.L. Wang, ACS Nano 10 (2016) 10366–10372.
[15] X. Liao, Q. Liao, Z. Zhang, X. Yan, Q. Liang, Q. Wang, M. Li, Y. Zhang, Adv. Funct. Mater. 26 (2016) 3074–3081.
[16] H. Xu, Y.F. Lu, J.X. Xiang, M.K. Zhang, Y.J. Zhao, Z.Y. Xie, Z.Z. Gu, Nanoscale 10 (2018) 2090–2098.
[17] H. Xu, J.X. Xiang, Y.F. Lu, M.K. Zhang, J.J. Li, B.B. Gao, Y.J. Zhao, Z.Z. Gu, ACS Appl. Mater. Interfaces 10 (2018) 11785–11793.
[18] C.C. Huang, Z.K. Kao, Y.C. Liao, ACS Appl. Mater. Interfaces 5 (2013) 12954–12959.
[19] S.Y. Hong, Y.H. Lee, H. Park, S.W. Jin, Y.R. Jeong, J. Yun, I. You, G. Zi, J.S. Ha, Adv. Mater. 28 (2016) 930–935.
[20] Y. Khan, M. Garg, Q. Gui, M. Schadt, A. Gaikwad, D. Han, N.A.D. Yamamoto, P. Hart, R. Welte, W. Wilson, S. Czarnecki, M. Poliks, Z. Jin, K. Ghose, F. Egitto, J. Turner, A.C. Arias, Adv. Funct. Mater. 26 (2016) 8764–8775.
[21] C. Pang, G.Y. Lee, T.I. Kim, S.M. Kim, H.N. Kim, S.H. Ahn, K.Y. Suh, Nat. Mater. 11 (2012) 795–801.
[22] W. Deng, T. Yang, L. Jin, C. Yan, H. Huang, X. Chu, Z. Wang, D. Xiong, G. Tian, Y. Gao, H. Zhang, W. Yang, Nano Energy 55 (2019) 516–525.
[23] J.H. Lee, J. Kim, D. Liu, F. Guo, X. Shen, Q. Zheng, S. Jeon, J.K. Kim, Adv. Funct. Mater. 29 (2019), 1901623.
[24] S. Cha, S.M. Kim, H. Kim, J. Ku, J.I. Sohn, Y.J. Park, B.G. Song, M.H. Jung, E.K. Lee, B.L. Choi, J.J. Park, Z.L. Wang, J.M. Kim, K. Kim, Nano Lett. 11 (2011) 5142–5147.
[25] D. Mandal, S. Yoon, K.J. Kim, Macromol. Rapid Commun. 32 (2011) 831–837.
[26] S. Siddiqui, D.-I. Kim, E. Roh, L.T. Duy, T.Q. Trung, M.T. Nguyen, N.-E. Lee, Nano Energy 30 (2016) 434–442.
[27] X. Wang, H. Zhang, L. Dong, X. Han, W. Du, J. Zhai, C. Pan, Z.L. Wang, Adv. Mater. 28 (2016) 2896–2903.
[28] J. Chun, N.-R. Kang, J.-Y. Kim, M.-S. Noh, C.-Y. Kang, D. Choi, S.-W. Kim, Z. Lin Wang, J. Min Baik, Nano Energy 11 (2015) 1–10.
[29] P.-K. Yang, Z.-H. Lin, K.C. Pradel, L. Lin, X. Li, X. Wen, J.-H. He, Z.L. Wang, ACS Nano 9 (2015) 901–907.
[30] Y.-T. Jao, P.-K. Yang, C.-M. Chiu, Y.-J. Lin, S.-W. Chen, D. Choi, Z.-H. Lin, Nano Energy 50 (2018) 513–520.
[31] X. Meng, Q. Cheng, X. Jiang, Z. Fang, X. Chen, S. Li, C. Li, C. Sun, W. Wang, Z. L. Wang, Nano Energy 51 (2018) 721–727.
[32] Sung-Ho Shin, Daehoon Park, Joo-Yun Jung, Min Hyung Lee Lee, Junghyo Nah, Department of Electrical Engineering, Chungnam National University, Yuseong-Gu, Daejeon 34134, Korea, Department of Nano Manufacturing Technology, Korea Institute of Machinery and Materials, Yuseong-Gu, Daejeon 34103, Korea, Department of Applied Chemistry, Kyung Hee University, Yongin, Gyeonggi 17104, Korea, Ferroelectric Zinc Oxide Nanowire Embedded Flexible Sensor for Motion and Temperature Sensing, ACS Appl. Mater. Interfaces 9 (11) (2017) 9233–9238, https://doi.org/10.1021/acsami.7b00380.
[33] Sung-Ho Shin, Yang Hyeog Kwon, Min Hyung Lee, Joo-Yun Jung, Jae Hun Seol, Junghyo Nah, Department of Electrical Engineering, Chungnam National University, Yuseong-Gu, Daejeon 34134, Korea, Department of Applied Chemistry, Kyung Hee University, Yongin, Gyeonggi 17104, Korea, Department of Nano Manufacturing Technology, Korea Institute of Machinery and Materials, Yuseong-Gu, Daejeon 34103, Korea, School of Mechatronics, Gwangju Institute of Science and Technology (GIST), Buk-Gu, Gwangju 61005, Korea, A vanadium-doped ZnO nanosheets–polymer composite for flexible piezoelectric nanogenerators, Nanoscale 8 (2016) 1314–1321, https://doi.org/10.1039/C5NR07185B.
[34] S. Jang, H. Kim, Y. Kim, B.J. Kang, J.H. Oh, Appl. Phys. Lett. 108 (2016), 143901.
[35] X. Wang, B. Yang, J. Liu, Y. Zhu, C. Yang, Q. He, Sci. Rep. 6 (2016) 36409.
[36] Z. Liang, R. Zhao, T. Qiu, R. Zou, Q. Xu, EnergyChem 1 (2019), 100001.
[37] X. Xiao, L. Zou, H. Pang, Q. Xu, Chem. Soc. Rev. 49 (2020) 301–331.
[38] G. Zhang, X. Xiao, B. Li, P. Gu, H. Xue, H. Pang, J. Mater. Chem. 5 (2017) 8155–8186.
[39] J. Ma, X. Guo, Y. Yan, H. Xue, H. Pang, Adv. Sci. 5 (2018), 1700986.
[40] G. Liu, Y. Sheng, J.W. Ager, M. Kraft, R. Xu, EnergyChem 1 (2019), 100014.
[41] J. Yu, X. Hou, J. He, M. Cui, C. Wang, W. Geng, J. Mu, B. Han, X. Chou, Nano Energy 69 (2020), 104437.
[42] C. Zhang, Y. Fan, H. Li, Y. Li, L. Zhang, S. Cao, S. Kuang, Y. Zhao, A. Chen, G. Zhu, Z.L. Wang, ACS Nano 12 (2018) 4803–4811.
[43] Y. Koshiba, M. Hirai, S. Horike, M. Morimoto, M. Misaki, T. Fukushima, K. Ishida, Sensor. Mater. 30 (2018) 2873–2879.
[44] S. Ghosh, H. Remita, L. Ramos, A. Dazzi, A. Deniset-Besseau, P. Beaunier, F. Goubard, P.-H. Aubert, F. Brisset, S. Remita, New J. Chem. 38 (2014) 1106–1115.

Md. Mehebub Alam received his M.Sc. and B.Sc. and Ph.D degree in physics from Jadavpur University in 2012, 2010 and 2018 respectively. He joined Chungnam National University as a postdoctoral researcher, S. Korea in 2018. He is currently working as a Postdoc at Linkoping University, Sweden. His research interest includes fabrication of piezo-, pyro and ferro-electric materials to design energy harvester and energy storage devices.

Sol Lee received his M.S. degree in Department of Electrical Engineering from Chungnam National University, Korea in 2020. He is currently Ph.D. student supervised by Professor Junghyo Nah. His research interests include triboelectric energy harvesting devices and novel air filter materials.

Minje Kim received his M.S. degree in Department of Electrical Engineering from Chungnam National University, Korea in 2020. He is currently Ph.D. student supervised by Professor Junghyo Nah. His research interests include triboelectric and piezoelectric energy harvesting devices.

Kyung Seok Han received his M.S. degree in Department of Electrical Engineering from Chungnam National University, Korea in 2020. He is currently Ph.D. student supervised by Professor Junghyo Nah. His research interests include piezoelectric energy harvesting devices and 3D printed sensors.

Viet Anh Cao received his M.S. degree in Faculty of Engineering Physics and Nanotechnology at University of Engineering and Technology, Vietnam National University, Ha Noi in 2017. He is a PhD student under the supervision of Professor Junghyo Nah in the Department of Electrical Engineering from Chungnam National University, Republic of Korea. His interests in research include the study of Triboelectric and piezoelectric energy harvesting devices, multifunctional sensors.

Junghyo Nah received Ph.D. in Electrical and Computer Engineering from the University of Texas at Austin in 2010. He worked as a postdoctoral scholar at University of California at Berkeley from 2011 to 2012. He joined the faculty of the Department of Electrical Engineering, Chungnam National University, Daejeon, Korea, in 2012. He is now a professor at this university. His research interests include piezoelectric and triboelectric energy harvesting devices, high performance air filter, and low dimensional semiconductor devices and sensors.